Origin of different piezoelectric responses in elemental Sb and Bi monolayers

Yunfei Hong,[1] Junkai Deng,[1,*] Qi Kong,[1] Yuefeng Yin,[2] Xiangdong Ding,[1] Jun Sun,[1] and Jefferson Zhe Liu[3,†]

[1]*State Key Laboratory for Mechanical Behavior of Materials, Xi'an Jiaotong University, Xi'an 710049, China*

[2]*Department of Materials Science and Engineering, Monash University, Clayton, Victoria 3800, Australia*

[3]*Department of Mechanical Engineering, The University of Melbourne, Parkville, Victoria 3010, Australia*

(Received 31 October 2023; revised 17 December 2023; accepted 8 January 2024; published 23 January 2024)

Sb and Bi monolayers, as single-element ferroelectric materials with similar atomic structure, hold intrinsic piezoelectricity theoretically, which makes them highly promising for applications in functional nanodevices such as sensors and actuators. Here, using density functional theory calculations, we systematically explore the piezoelectric response of Sb and Bi monolayers. Our findings reveal that Sb exhibits a negative piezoelectric response, whereas Bi displays a positive one. This discrepancy is attributed to the dominant role of different atomic internal distortions (internal-strain terms) in response to applied strain. Further electron-density distribution analysis reveals that the atomic bonding in Sb tends to be covalent, while the atomic bonding in Bi leans more towards ionic. Compared to the Sb monolayer, the Bi monolayer is distinguished by its more pronounced lone-pair orbitals electrons and associated larger Born effective charges. The Coulomb repulsions between lone-pair orbitals electrons and the chemical bonds lead to the Bi monolayer possessing more prominent atomic folds and, consequently, more significant atomic distortion in the z direction under strain. These differences result in a considerable difference in internal-strain terms, ultimately leading to the reversed piezoelectric response between Sb and Bi monolayers. The present work provides valuable insights into the piezoelectric mechanism of two dimensional ferroelectric materials and their potential applications in nanoelectronic devices.

DOI: 10.1103/PhysRevB.109.035204

I. INTRODUCTION

Piezoelectric materials, due to their ability to be electrically polarized under an externally applied strain and, conversely, to be deformed by an applied voltage, provide an effective means of transducing signals between mechanical strain and electrical polarization. Piezoelectric materials have widespread applications in electromechanical systems and electronic devices such as energy harvesters, pressure sensors, actuators, strain-tuned electronics, and optoelectronics [1–3]. The piezoelectric performance of materials is quantified by the piezoelectric coefficients. In most cases, the piezoelectric coefficients are positive, indicating that polarization is more likely to increase under mechanical stretching [4,5]. However, in recent years, researchers have discovered some exceptions where certain materials exhibit anomalous negative piezoelectric responses. For instance, the ferroelectric polymer polyvinylidene fluoride (PVDF) and its copolymers exhibit negative longitudinal piezoelectric coefficients [6–9]. In addition, theoretical predictions suggest the presence of significant negative piezoelectric responses in some specific organic molecular ferroelectrics [10], hexagonal *ABC* ferroelectrics [11], layered van der Walls ferroelectrics [12–14], group IV-V MX_2 [15,16], HfO_2 ferroelectric [17,18], and sphalerite compounds [19–21].

The piezoelectric effect originates from the electric charge redistribution under externally applied strains, involving relative ion displacement and the changes in Born effective charges. As a result, the total piezoelectric coefficient (e_{22}) can be decomposed into the clamped-ion term (e^0_{22}) and the internal-strain term (e'_{22}) [22]. Recently, Qi *et al.* discovered lag of the Wannier center effect that results from the decay of the Coulombic repulsion between electrons with the separation of anions and cations [13]. The Wannier centers generally fail to follow the anions (in fractional coordinates) completely upon a tensile strain, contributing to the consistently negative clamped-ion term (e^0_{22}) in piezoelectric materials. The competition between these two terms determines the sign (positive or negative) of the piezoelectric coefficient. In the case of hexagonal *ABC* ferroelectrics, the negative clamped-ion term (e^0_{22}) dominates over the internal-strain term (e'_{22}), leading to the overall negative piezoelectric coefficients [11]. However, this general principle offers limited insights and clues to determine the negative or positive piezoelectric responses that could be used for material design.

With the fast advances of miniaturized electronic devices, two-dimensional (2D) piezoelectric materials have drawn great interest [23,24]. Many 2D piezoelectric materials have been successfully predicted, with some of the predicted materials being synthesized in experiments [5,25–29]. The Sb and Bi ferroelectric monolayers, as unique single-element ferroelectric materials [29–34], have attracted significant attention. The ferroelectric nature of Sb and Bi monolayers enables their intrinsic piezoelectricity. Note that unlike the traditional piezoelectric compounds, where ions primarily contribute the

*Corresponding author: junkai.deng@mail.xjtu.edu.cn

†Corresponding author: zhe.liu@unimelb.edu.au

polarization, the polarization in Sb and Bi monolayers arises solely from the electron contribution. The electron cloud redistribution under applied strains exclusively determines the piezoelectric response. Since the electron redistribution behavior could be highly flexible and closely related to the elemental species, crystal structure, and bonding types [35,36], an in-depth understanding of the piezoelectric response of Sb and Bi monolayers is of great significance for exploring their electromechanical coupling properties and elucidating their physical mechanisms.

In this paper, we investigate the piezoelectric response of Sb and Bi monolayers using density functional theory calculations. Despite their identical crystal symmetry ($Pmn2_1$), our DFT results reveal an unexpected contrast: the Bi monolayer exhibits positive piezoelectricity, while Sb exhibits negative piezoelectricity. By decomposing the piezoelectric coefficient into clamping-ion (e^0_{22}) and internal-strain (e'_{22}) terms, we find that the internal-strain term determines the difference. Furthermore, we unravel the physical mechanism of the polarization change during the internal strain process using the density of states (DOS), Born effective charges, and atomic displacement calculations. This work can provide deep insight into the mechanism of piezoelectricity and can be used to design potential devices employing the anomalous electromechanical response.

II. METHODS

Our density functional theory (DFT) calculation were performed using the Vienna *Ab-initio* Simulation Package (VASP) [37–40]. The Perdew-Burke-Ernzerhof (PBE) exchange-correlation functional [41] and the projected augmented plane-wave method were adopted. The monolayer is placed in the x-y plane. The periodic boundary condition was applied along all three directions. A vacuum space of about 20 Å was used along the z axis to avoid artificial interaction. The valence configuration is $5s^25p^3$ for Sb. For Bi, the valence configuration is $6s^26p^35d^{10}$. The spin-orbit coupling (SOC) was considered in all calculations [42–44]. The energy cutoff was set to be 500 eV. The Brillouin zone was sampled in k space within $15 \times 15 \times 1$ mesh for Sb and Bi monolayers. The positions of all atoms were fully relaxed until the energy between two consecutive steps was less than 10^{-6} eV, and the maximum force was 0.001 eV/Å on each atom. The Poisson's ratio effect [45–47] was considered when applying uniaxial strain. The electric polarization was computed using the Berry-phase method [48,49].

III. RESULTS AND DISCUSSION

Sb and Bi monolayers are crystallized in the asymmetric washboard structures with space group $Pmn2_1$ and four atoms per unit cell. The Sb and Bi monolayers have been predicted as single-elemental ferroelectric materials, which was later experimentally confirmed for the Bi monolayer in 2023 [29]. In contrast to black phosphorus, which has only one chemical bonding state, the asymmetric washboard structure of Sb and Bi monolayers allows for different chemical surroundings, enabling the adoption of two bonding states in these elemental materials.

TABLE I. The piezoelectric tensor elements e_{22} of Sb and Bi monolayers. e_{22} is decomposed into the "clamped-ion" term (e^0_{22}) and the "internal-strain" term (e'_{22}).

	$e^0_{22}(\times10^{-10}\text{c/m})$	$e'_{22}(\times10^{-10}\text{c/m})$	$e_{22}(\times10^{-10}\text{c/m})$
Sb	−2.623	0.652	−1.971
Bi	−2.157	9.810	7.653

The optimized lattice constants of Sb and Bi monolayers are $a = 4.362$ Å, $b = 4.736$ Å, and $a = 4.581$ Å, $b = 4.913$ Å, respectively (Fig. 1). The Sb and Bi monolayers possessed a stable structure, as confirmed by the phonon spectrum (Fig. S1 of the Supplemental Material [50]). Our DFT calculations show that the 2D Sb is a direct band gap semiconductor (with a band gap of 0.22 eV), while the 2D Bi is an indirect band gap semiconductor (with a band gap of 0.26 eV). The energy band structure shows that the atomic buckling of Sb and Bi monolayers splits the energy level of two p_z orbitals, resulting in two states in one element. In the case of the Sb monolayer [Fig. 1(c)], the conduction band and valence band at the Γ point are mainly contributed by p_z orbitals of Sb^+ and Sb^- atoms, respectively. The p_z orbitals of Sb^- are occupied and the p_z orbitals of Sb^+ are empty, indicating the electron transfer from Sb^+ to Sb^-. The unit cell of the Sb monolayer contains two sublayers and each sublayer has one Sb^- atom and one Sb^+ atom. Similarly, electron transfer also occurs in Bi monolayer [Fig. 1(d)].

The Berry phase calculation results show that the spontaneous polarizations along the y direction of Sb and Bi monolayers are −38 pc/m and −43 pc/m, respectively. The z coordinates of $Sb^+(Bi^+)$ and $Sb^-(Bi^-)$ atoms are significantly different, leading to the considerable tilting of Sb-Sb bonding within the sublayer. This is different from nonpolarized black phosphorene (space group $Pmna$), where the z coordinates of the P atoms within a sublayer are identical [51]. Thus, when the Sb and Bi monolayers (with the space group of $Pmn2_1$) were transformed to a high-symmetric structure, the same as the phosphorene ($Pmna$), eliminating the difference in z coordinates could give rise to the nonpolarization state. It is confirmed by removing the energy level splitting of the two p_z orbitals in such a high-symmetric structure (Fig. S2 [50]), indicating one chemical bonding state only. Thus, the spontaneous polarization of Sb (Bi) was highly dependent on the z coordinates of atoms.

To quantify the piezoelectric response of Sb and Bi monolayers, the polarization changes with uniaxial strain (−0.5% to 0.5%) in the polarization direction (y) were determined as shown in Figs. 2(a) and 2(b), respectively. The polarization response to fully relaxed Sb and Bi monolayers under different strains is fitted into straight lines. Their slopes are the piezoelectric tensor elements (e_{22}) for full structural relaxation. As reported in Table I, the e_{22} is negative (-1.971×10^{-10} c/m) for Sb and positive (7.653×10^{-10} c/m) for Bi, indicating completely reversed piezoelectric responses despite a similar structure.

As shown in Table SIII and Fig. S3 of the Supplemental Material [50], the results show that the piezoelectric coefficients are insensitive to the strain range for Sb monolayer.

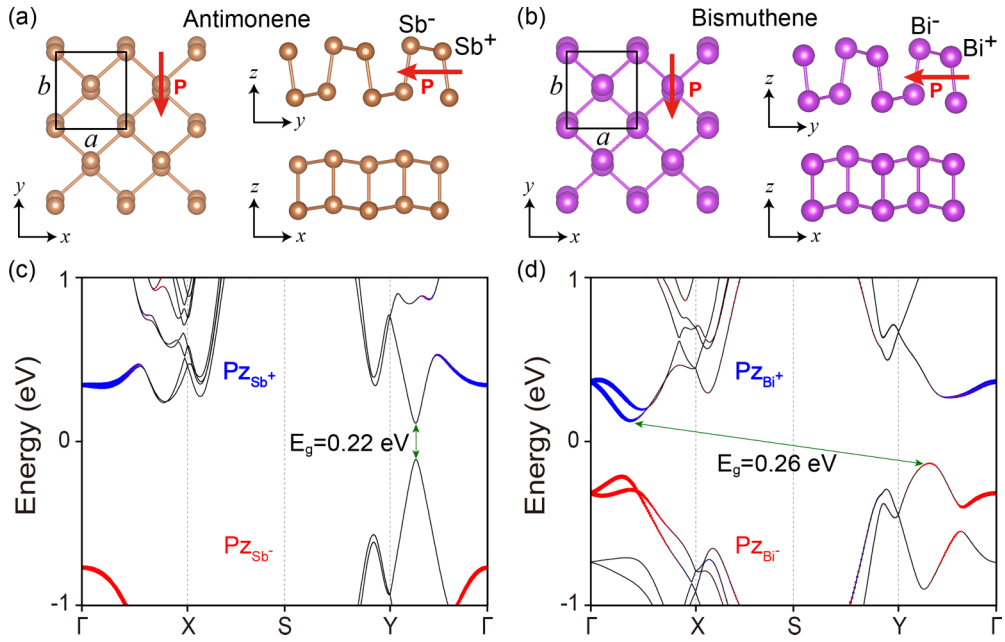

FIG. 1. Crystal structure and electronic properties of Sb and Bi 2D monolayers. (a),(b) The crystal structure of Sb and Bi monolayers. Solid line boxes represent the unit cell of Sb and Bi. The red arrows indicate the intrinsic polarization direction. (c),(d) The electronic band structures of Sb and Bi monolayers. The size of red (blue) circles represents the contributions of the p_z orbitals of Sb^- (Sb^+) and Bi^-(Bi^+). The valance band maximum (VBM) and conduction band minimum (CBM) were identified as the end of green arrows. The energy difference of them was the band gap (E_g).

However, due to the nonlinear piezoelectric response, discussed in the Supplemental Material [50], the piezoelectric coefficients between two strain ranges show more significant differences for Bi monolayer, despite both being positive. This paper focuses on whether the piezoelectric response is positive or negative instead of their magnitude. Therefore, the piezoelectric response in a small strain range (−0.5% to 0.5%) was discussed.

In modern piezoelectric theory, the total piezoelectric coefficient (e_{22}) can be decomposed into the clamped-ion term (e^0_{22}) and the internal-strain term (e'_{22}) [22],

$$e_{22} = e^0_{22} + e'_{22}. \tag{1}$$

The e^0_{22} value can be computed with the internal atomic fractional coordinates fixed at their zero-strain states, corresponding to the uniform scaling of the atomic positions in the unit cell as the strain state is changed. This clamped-ion piezoelectric coefficient features the change of Born effective charges, reflecting the redistribution of electrons with respect to a homogeneous strain.

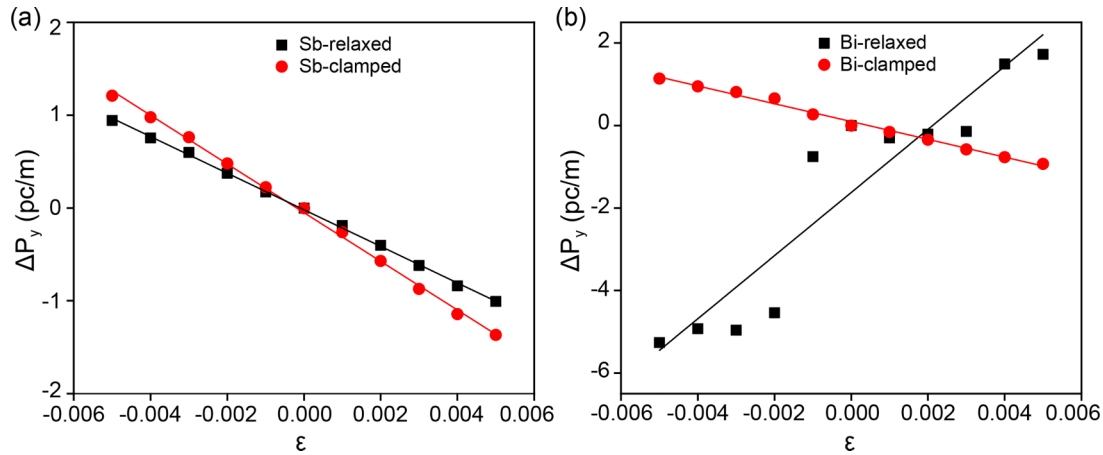

FIG. 2. The polarization of Sb (a) and Bi (b) as a function of uniaxial strain. "$\varepsilon = 0$" represents the ground states of Sb and Bi monolayers. The slopes of Sb/Bi-relaxed curves are the total piezoelectric coefficient (e_{22}) of Sb/Bi monolayers. The slopes of Sb/Bi-clamped curves are the clamped-ion terms (e^0_{22}) of Sb/Bi monolayers.

The internal-strain term e'_{22} originates from the internal microscopic polar distortion in response to a microscopic strain applied in the y direction [(Eq. (2)],

$$e'_{22} = \sum_s \frac{e}{V}\left(Z^*_{12}\frac{a\times\partial\mu_1(s)}{\partial\eta_2} + Z^*_{22}\frac{b\times\partial\mu_2(s)}{\partial\eta_2} + Z^*_{32}\frac{c\times\partial\mu_3(s)}{\partial\eta_2}\right), \quad (2)$$

where μ_1, μ_2, and μ_3 represent the fractional atomic coordinates and η_2 denotes the macroscopic strain applied in the y direction. The summation runs over the atoms (s) in the unit cell of Sb (Bi). V represents the volume (in 3D systems) or area (in 2D systems) of the unit cell. The parameter e represents electron charge, and a, b, and c are the lattice constants. The Born effective charges related to the displacement of μ_1, μ_2, and μ_3 are Z^*_{12}, Z^*_{22}, and Z^*_{32}. The internal-strain term mainly reflects the polarization change from the internal atomic distortion. Due to the change of Born effective charge values, the internal-strain term is difficult to calculate directly. It is usually obtained by subtracting the clamped-ion term from the total piezoelectric coefficient.

The results of the clamped-ion (e^0_{22}) and internal-strain (e'_{22}) terms are summarized in Table I. The clamped-ion term for Sb (-2.623×10^{-10} c/m) and Bi (-2.157×10^{-10} c/m) are both negative with a similar magnitude. Note that due to the lag of Wannier centers effect, the clamped-ion term should always be negative [13]. The similar magnitude could be attributed to their similar crystal structures. The internal-strain term values for Sb and Bi are both positive but with a significantly different magnitude, i.e., 0.652×10^{-10} c/m for Sb and 9.810×10^{-10} c/m for Bi. The internal-strain term for Bi is over ten times larger than that of Sb. Consequently, the piezoelectric effect of the Sb monolayer is negative, as the negative clamped-ion piezoelectric response dominates over the internal-strain contribution. On the other hand, the piezoelectric response of Bi is dominated by the internal-strain term, resulting in a positive piezoelectric effect. The clamped-ion term is not responsible for the reversed piezoelectric coefficients of Sb and Bi, but rather the internal-strain term.

We also calculated the Wannier functions using the WANNIER90 code [52,53]. The band structure calculated by WANNIER90 overlapped with that by DFT, as shown in Fig. S4 [50], showing the high-quality Wannier functions. For the Sb monolayer, the intrinsic polarization calculated by WANNIER90 was -35.89 pc/m, close to our Berry phase calculation (-38 pc/m). The total piezoelectric coefficient (e_{22}) was -0.24×10^{-10} c/m and the clamped-ion term (e^0_{22}) was -3.46×10^{-10} c/m (Table SI [50]), showing the negative piezoelectric response dominated by the negative clamped-ion term. When the tensile strain was applied, the Wannier center moved from 0.47 Å (-0.5%) to 0.44 Å (0.5%), resulting in the negative clamped-ion term. However, the polarization of the Bi monolayer calculated by WANNIER90 was 2.77 pc/m, which was different from the results of our Berry phase calculation (-43 pc/m). It was found that the polarization was sensitive to the "*dis_froz_max*" parameter (Table SII [50]). We cannot get a reliable calculated polarization value that is close to the experiment (-41 pc/m) [29]. This could be due to the strong spin-orbit coupling of Bi, which brings great challenges to calculating Wannier functions. In contrast, our Berry phase results were close to the recent experiment and other DFT calculations [32]. Wannier functions may not be suitable for calculating polarization and piezoelectric response of 2D Bi.

TABLE II. The Born effective charges of Sb and Bi monolayers (the ground state). Sb^- (Bi^-) and Sb^+ (Bi^+) are two states of 2D Sb (Bi). By taking symmetry into account, the values were averaged and normalized.

	Z^*_{12} (e)	Z^*_{22} (e)	Z^*_{32} (e)
Sb^-	−0.10	−0.34	−0.29/0.29
Sb^+	0.10	0.34	−0.84/0.84
Bi^-	0.09	−0.74	−0.07/0.07
Bi^+	−0.09	0.74	−3.28/3.28

According to Eq. (2), the products of Born effective charges and atomic displacements play important roles in polarization and the internal-strain term of piezoelectric coefficient. The Born effective charges of Sb and Bi are calculated and summarized in Table II. Due to the symmetry breaking, the Born effective charges (Z^*_{32}) of two atoms in the same state are reversed. The absolute values of Z^*_{32} for Sb^- ($0.29e$) and Sb^+ ($0.84e$) are quite different, indicating the transfer of electrons between atoms. A similar behavior was also observed in Bi monolayer. In addition, the difference between Z^*_{32} for positive and negative charged atoms within Bi monolayer ($0.07e$ and $3.28e$) is much more significant than that of Sb monolayer, indicating that more electrons transfer from Bi^+ to Bi^-. More importantly, the Born effective charges Z^*_{22} of Bi are more than twice as large as those of Sb, and the Z^*_{32} of Bi^+ is almost four times as large as Sb^+, suggesting that the polarization of 2D Bi would change more significantly at the same atomic displacement.

According to Eq. (2), the atomic displacement (μ_i) under uniaxial strain also plays an important role in the internal-strain term. Since the Born effective charges and atomic displacements in the x direction are almost zero, they are not considered in this work (Table II). The displacement in the y and z directions may play a major role in the change of polarization. The structural parameters under uniaxial strain are measured, as shown in Fig. 3. When the strain was applied in the y direction, the lattice constant b can be decomposed into y_1 and y_2 ($y_1 + y_2 = 0.5b$), as shown in Figs. 3(a) and 3(b). Figures 3(c) and 3(d) show that the y_2 component always changed faster than y_1 both in Sb and Bi monolayer. This suggests that rotating chemical bonds between sublayers is easier than extending chemical bonds within a sublayer. During the clamped-ion process, all chemical bonds extend or shorten together proportionally, resulting from the homogeneous strain. However, during the internal-strain process (internal stress release), the y_1 decreased while the y_2 increased, and the lattice constant b was fixed [Figs. 3(e) and 3(f)]. Meanwhile, the atomic displacements of Sb are about two times larger than that of Bi. The Born effective charges Z^*_{22} of Sb are about half as large as those of Bi. As a result, the products of Z^*_{22} and atomic displacement of Sb and Bi have similar values,

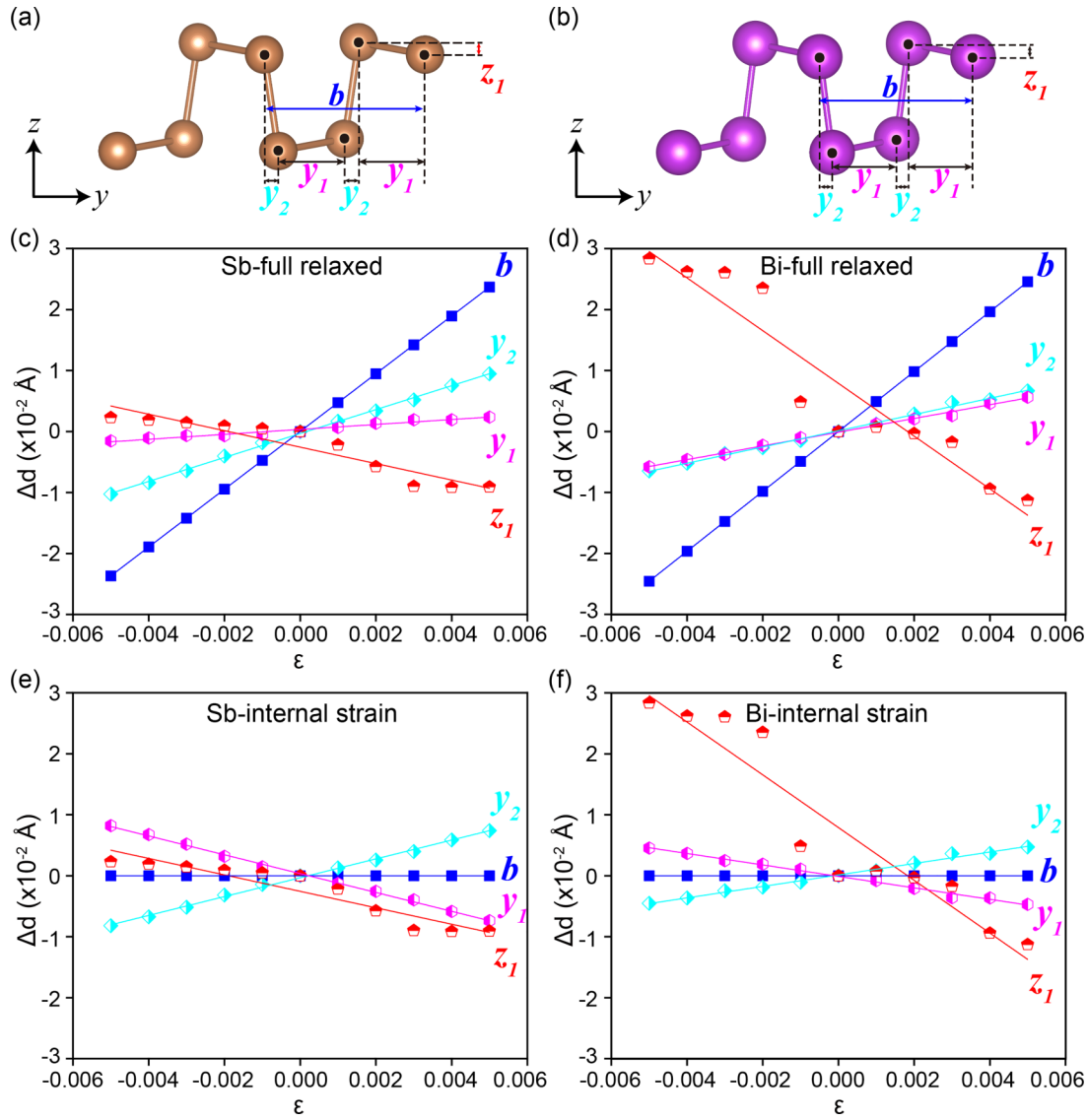

FIG. 3. Changes of structural parameters of Sb and Bi under uniaxial strain. (a),(b) Crystal structure of Sb and Bi. The parameter b is the lattice constant in the y direction. y_1 and y_2 represent distances between adjacent atoms in the y direction, and the sum of y_1 and y_2 is equal to half the lattice constant b ($y_1 + y_2 = 0.5b$). The parameter z_1 represents the distance between $Sb^-(Bi^-)$ and $Sb^+(Bi^+)$ atoms in the z direction. (c),(d) Changes of fully relaxed structural parameters of Sb and Bi. (e),(f) Changes of structural parameters of Sb and Bi during the internal-strain process.

indicating that the y direction displacement is not responsible for the huge difference in the internal-strain terms (e'_{22}).

Furthermore, the structural parameter z_1 [defined as the z-coordinate difference of $Sb^+(Bi^+)$ and $Sb^-(Bi^-)$ atoms] also decreases in both Sb and Bi when the stretching is applied in the y direction [Figs. 3(c) and 3(d)]. During the clamped-ion process, the z_1 is constant and equal to the value of the ground state, resulting from the protection of the z-direction vacuum layer. Thus, the displacement in the z direction only occurred during the internal-strain process. As shown in Figs. 3(e) and 3(f), the z_1 of Bi always changed faster than that of Sb and the atomic displacement of Bi is about four times larger than that of Sb in the same strain. Besides, the Born effective charges Z^*_{32} of Bi are also about four times larger than those of Sb, making the product of Z^*_{32} and displacements of Bi over ten times larger than that of Sb. As a result, the internal-strain term (e'_{22}) of Bi is one order of magnitude larger than that of Sb. The z-direction displacement and Z^*_{32} play a dominant role in the internal-strain term of Sb and Bi monolayers.

To explore the mechanism of Born effective charge differences between Sb and Bi monolayers, the density of states (DOS) was calculated to analyze their electronic structure (Fig. 4). The first peak of Sb^- (Bi^-) near the valence band maximum (VBM) is higher than that of $Sb^+(Bi^+)$ atom, as highlighted in the figure by red boxes, indicating the electron transfer from $Sb^+(Bi^+)$ to Sb^- (Bi^-). The electron-density distributions in the energy range of the first peak (−0.9 to 0 eV for Sb and −0.35 to 0 eV for Bi) exhibit distinct differences between Sb and Bi. In particular, the electron-density distribution of Bi is more localized than that of Sb. When comparing the electron-density distributions in the energy range of the second peak (−1.4 to −0.9 eV for Sb and −1.0 to

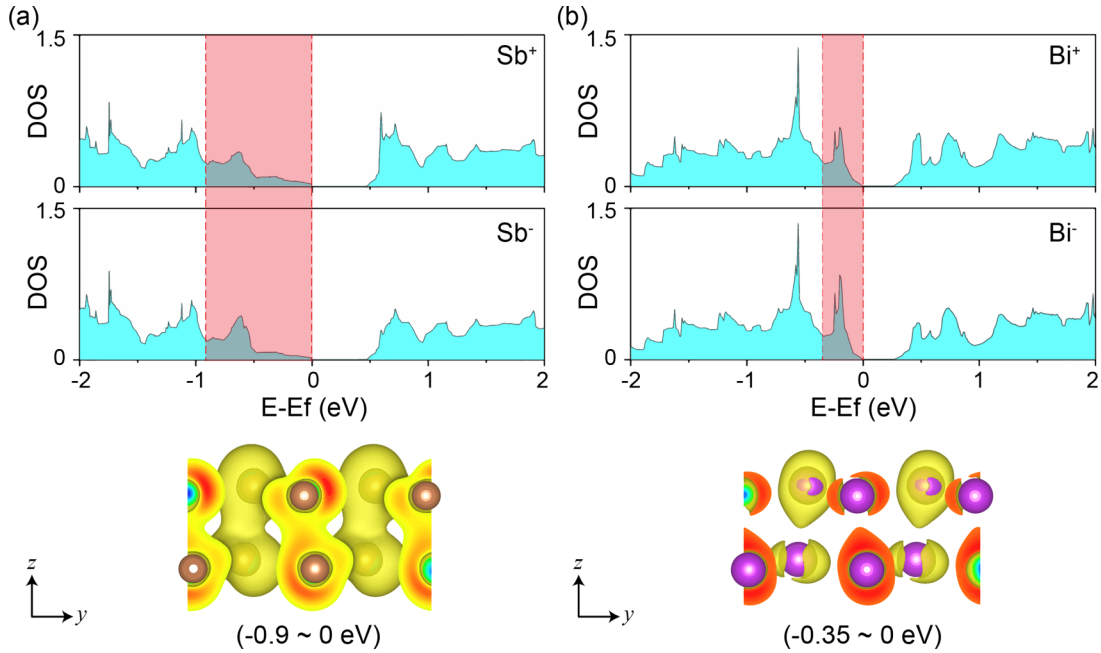

FIG. 4. Bonding analysis of Sb (a) and Bi (b) monolayers. The density of states of Sb^+ (Bi^+) and Sb^- (Bi^-) versus $E - E_f$ are shown in light blue, where E_f denotes Fermi level. The red boxes highlight the difference in DOS between the two atoms near the valence band maximum, and the electron-density distribution (isosurfaces = 0.0007 e/bohr^3) in this energy range are visualized in the bottom subfigures.

−0.35 eV for Bi), there is no significant difference (Fig. S5 [50]). It can be concluded that the electron-density distribution of the first peak primarily reflects the difference in bonding between the two materials.

The first peak of the Bi monolayer is narrower and higher than that of Sb, indicating the electron-density distribution is more localized, which is also reflected in the charge distribution plot, as shown in the comparison of the bottom subfigures in Fig. 4. The electrons of Bi are predominantly localized within each single atom and appear like lone-pair orbitals, displaying the characteristics of ionic bonding. In contrast, some electrons of Sb are shared among neighboring atoms, exhibiting the characteristics of covalent bonds. Consequently, the Born effective charges of Bi are larger than those of Sb, resulting in the reversed piezoelectric response ultimately. The results suggest that negative piezoelectric effect is more likely to occur in covalent piezoelectrics which was also concluded in wurtzite piezoelectric semiconductors [54].

Furthermore, the pronounced lone-pair orbitals electrons around Bi^- atoms [electron localization function (ELF) analysis shown in Fig. S6 [50]] may be related to the intrinsic folds (z_1) of Bi. The Coulomb repulsion between the lone-pair orbital electrons and the surrounding chemical bonds drives the Bi^- away from Bi^+, creating the large intrinsic folds (z_1) of Bi [45,55]. The large intrinsic fold allows Bi atoms to undergo more significant displacements along the z axis under uniaxial strain.

IV. CONCLUSION

In this work, using DFT calculations, we found unexpected reversed piezoelectric response of Sb and Bi that have similar crystal structure. The Sb has a negative piezoelectric coefficient (e_{22}), whereas Bi has a positive one. Our analysis shows ten times differences of internal-strain terms e'_{22}, which plays the dominant role in their reversed piezoelectric response. In-depth electronic structure analysis revealed that the chemical bond of Bi is predominantly ionic, whereas the chemical bond of Sb is more covalent. This difference results in Bi having larger Born effective charges than Sb. Furthermore, the lone-pair electrons of Bi create more prominent folds and z-direction displacements. Consequently, the positive internal-strain term of Bi is much larger than that of Sb, dominating the piezoelectric coefficient. In contrast, the piezoelectric coefficient of Sb is dominated by the negative clamped-ion term. This work provides valuable insights into the piezoelectric mechanism of Sb and Bi monolayer materials and potential applications in nanodevices using their anomalous electromechanical response.

ACKNOWLEDGMENTS

The authors gratefully acknowledge the support of NSFC (Grant No. 11974269), the support by the Key Research and Development Program of Shaanxi (Grant No. 2023-YBGY-480), and the 111 projects 2.0 (Grant No. BP0618008). J.Z.L. acknowledges the support from ARC discovery projects (Grant No. DP210103888) and HPC from National Computational Infrastructure from Australia. The authors also thank F. Yang and X. D. Zhang at the Network Information Center of Xi'an Jiaotong University for supporting the HPC platform. This work was also supported by State Key Laboratory for Mechanical Behavior of Materials.

[1] M. C. Sekhar, E. Veena, N. S. Kumar, K. C. B. Naidu, A. Mallikarjuna, and D. B. Basha, A review on piezoelectric materials and their applications, Cryst. Res. Technol. **58**, 2200130 (2023).

[2] H. Liu, J. Zhong, C. Lee, S.-W. Lee, and L. Lin, A comprehensive review on piezoelectric energy harvesting technology: materials, mechanisms, and applications, Appl. Phys. Rev. **5**, 041306 (2018).

[3] B. Watson, J. Friend, and L. Yeo, Piezoelectric ultrasonic micro/milli-scale actuators, Sens. Actuators Phys. **152**, 219 (2009).

[4] K. Lefki and G. J. M. Dormans, Measurement of piezoelectric coefficients of ferroelectric thin films, J. Appl. Phys. **76**, 1764 (1994).

[5] M. N. Blonsky, H. L. Zhuang, A. K. Singh, and R. G. Hennig, Ab initio prediction of piezoelectricity in two-dimensional materials, ACS Nano **9**, 9885 (2015).

[6] V. S. Bystrov, E. V. Paramonova, I. K. Bdikin, A. V. Bystrova, R. C. Pullar, and A. L. Kholkin, Molecular Modeling of the piezoelectric effect in the ferroelectric Polymer Poly(Vinylidene Fluoride) (PVDF), J. Mol. Model. **19**, 3591 (2013).

[7] I. Katsouras, K. Asadi, M. Li, T. B. van Driel, K. S. Kjær, D. Zhao, T. Lenz, Y. Gu, P. W. M. Blom, D. Damjanovic, M. M. Nielsen, and D. M. de Leeuw, The negative piezoelectric effect of the ferroelectric polymer poly(vinylidene fluoride), Nat. Mater. **15**, 78 (2016).

[8] T. Furukawa, J. X. Wen, K. Suzuki, Y. Takashina, and M. Date, Piezoelectricity and pyroelectricity in vinylidene fluoride/trifluoroethylene copolymers, J. Appl. Phys. **56**, 829 (1984).

[9] Y. Liu and Q. Wang, Ferroelectric polymers exhibiting negative longitudinal piezoelectric coefficient: progress and prospects, Adv. Sci. **7**, 1902468 (2020).

[10] I. Urbanaviciute, X. Meng, M. Biler, Y. Wei, T. D. Cornelissen, S. Bhattacharjee, M. Linares, and M. Kemerink, Negative piezoelectric effect in an organic supramolecular ferroelectric, Mater. Horiz. **6**, 1688 (2019).

[11] S. Liu and R. E. Cohen, Origin of negative longitudinal piezoelectric effect, Phys. Rev. Lett. **119**, 207601 (2017).

[12] L. You, Y. Zhang, S. Zhou, A. Chaturvedi, S. A. Morris, F. Liu, L. Chang, D. Ichinose, H. Funakubo, W. Hu, T. Wu, Z. Liu, S. Dong, and J. Wang, Origin of giant negative piezoelectricity in a layered van Der Waals ferroelectric, Sci. Adv. **5**, eaav3780 (2019).

[13] Y. Qi and A. M. Rappe, Widespread negative longitudinal piezoelectric responses in ferroelectric crystals with layered structures, Phys. Rev. Lett. **126**, 217601 (2021).

[14] J. Kim, K. M. Rabe, and D. Vanderbilt, Negative piezoelectric response of van Der Waals layered bismuth tellurohalides, Phys. Rev. B **100**, 104115 (2019).

[15] Y. Xu, Z. Li, C. He, J. Li, T. Ouyang, C. Zhang, C. Tang, and J. Zhong, Intrinsic piezoelectricity of monolayer group IV–V MX_2: SiP_2, $SiAs_2$, GeP_2, and $GeAs_2$, Appl. Phys. Lett. **116**, 023103 (2020).

[16] Y. Zhao, G. Gou, X. Lu, and Y. Hao, Intrinsic auxeticity and negative piezoelectricity in two-dimensional group-iv dipnictide monolayers with in-plane anisotropy, J. Mater. Chem. C **9**, 6068 (2021).

[17] J. Liu, S. Liu, L. H. Liu, B. Hanrahan, and S. T. Pantelides, Origin of pyroelectricity in ferroelectric HfO_2, Phys. Rev. Appl. **12**, 034032 (2019).

[18] J. Liu, S. Liu, J.-Y. Yang, and L. Liu, Electric auxetic effect in piezoelectrics, Phys. Rev. Lett. **125**, 197601 (2020).

[19] F. Bernardini, V. Fiorentini, and D. Vanderbilt, Spontaneous polarization and piezoelectric constants of III-V nitrides, Phys. Rev. B **56**, R10024(R) (1997).

[20] K. S. Suzuki and H. O. H. Okumura, First-principles study on piezoelectric constants in strained BN, AlN, and GaN, Jpn. J. Appl. Phys. **37**, L1421 (1998).

[21] K. Shimada, First-principles determination of piezoelectric stress and strain constants of wurtzite III–V nitrides, Jpn. J. Appl. Phys. **45**, L358 (2006).

[22] G. Sághi-Szabó, R. E. Cohen, and H. Krakauer, First-principles study of piezoelectricity in $PbTiO_3$, Phys. Rev. Lett. **80**, 4321 (1998).

[23] C. Cui, F. Xue, W.-J. Hu, and L.-J. Li, Two-dimensional materials with piezoelectric and ferroelectric functionalities, npj 2D Mater. Appl. **2**, 18 (2018).

[24] Y. Peng, M. Que, J. Tao, X. Wang, J. Lu, G. Hu, B. Wan, Q. Xu, and C. Pan, Progress in piezotronic and piezo-phototronic effect of 2D materials, 2D Mater. **5**, 042003 (2018).

[25] K.-A. N. Duerloo, M. T. Ong, and E. J. Reed, Intrinsic piezoelectricity in two-dimensional materials, J. Phys. Chem. Lett. **3**, 2871 (2012).

[26] M. T. Ong and E. J. Reed, Engineered piezoelectricity in graphene, ACS Nano **6**, 1387 (2012).

[27] W. Wu, L. Wang, Y. Li, F. Zhang, L. Lin, S. Niu, D. Chenet, X. Zhang, Y. Hao, T. F. Heinz, J. Hone, and Z. L. Wang, Piezoelectricity of single-atomic-layer MoS_2 for energy conversion and piezotronics, Nature (London) **514**, 470 (2014).

[28] R. Fei, W. Li, J. Li, and L. Yang, Giant piezoelectricity of monolayer group IV monochalcogenides: SnSe, SnS, GeSe, and GeS, Appl. Phys. Lett. **107**, 173104 (2015).

[29] J. Gou, H. Bai, X. Zhang, Y. L. Huang, S. Duan, A. Ariando, S. A. Yang, L. Chen, Y. Lu, and A. T. S. Wee, Two-dimensional ferroelectricity in a single-element bismuth monolayer, Nature (London) **617**, 67 (2023).

[30] C. Xiao, F. Wang, S. A. Yang, Y. Lu, Y. Feng, and S. Zhang, Elemental ferroelectricity and antiferroelectricity in group-V monolayer, Adv. Funct. Mater. **28**, 1707383 (2018).

[31] Y. Guo, H. Zhu, and Q. Wang, Large second harmonic generation in elemental α-Sb and α-Bi monolayers, J. Phys. Chem. C **124**, 5506 (2020).

[32] Y. Pan and J. Zhou, Toggling valley-spin locking and nonlinear optical properties of single-element multiferroic monolayers via light, Phys. Rev. Appl. **14**, 014024 (2020).

[33] Z. Qian, J. Zhou, H. Wang, and S. Liu, Shift current response in elemental two-dimensional ferroelectrics, npj Comput. Mater. **9**, 67 (2023).

[34] Y. Hong, J. Deng, X. Ding, J. Sun, and J. Z. Liu, Size limiting elemental ferroelectricity in Bi nanoribbons: Observation, mechanism, and opportunity, J. Phys. Chem. Lett. **14**, 3160 (2023).

[35] E. V. Tsiper and Z. G. Soos, Charge redistribution and polarization energy of organic molecular crystals, Phys. Rev. B **64**, 195124 (2001).

[36] P. Sadhukhan, S. Q. Wu, J. I. Long, T. Nakanishi, S. Kanegawa, K. Gao, K. Yamamoto, H. Okajima, A. Sakamoto, M. L. Baker,

T. Kroll, D. Sokaras, A. Okazawa, N. Kojima, Y. Shiota, K. Yoshizawa, and O. Sato, Manipulating electron redistribution to achieve electronic pyroelectricity in molecular [FeCo] crystals, Nat. Commun. **12**, 4836 (2021).

[37] P. Hohenberg and W. Kohn, Inhomogeneous electron gas, Phys. Rev. **136**, B864 (1964).

[38] W. Kohn and L. J. Sham, Self-consistent equations including exchange and correlation effects, Phys. Rev. **140**, A1133 (1965).

[39] G. Kresse and J. Hafner, Ab initio molecular dynamics for liquid metals, Phys. Rev. B **47**, 558 (1993).

[40] G. Kresse and J. Furthmüller, Efficiency of ab-initio total energy calculations for metals and semiconductors using a plane-wave basis set, Comput. Mater. Sci. **6**, 15 (1996).

[41] J. P. Perdew, K. Burke, and M. Ernzerhof, Generalized gradient approximation made simple, Phys. Rev. Lett. **77**, 3865 (1996).

[42] M. Blume and R. E. Watson, Theory of spin-orbit coupling in atoms I. Derivation of the spin-orbit coupling constant, Proc. R. Soc. A **270**, 127 (1962).

[43] V. Galitski and I. B. Spielman, Spin–orbit coupling in quantum gases, Nature (London) **494**, 49 (2013).

[44] A. Manchon, H. C. Koo, J. Nitta, S. M. Frolov, and R. A. Duine, New perspectives for rashba spin–orbit coupling, Nat. Mater. **14**, 871 (2015).

[45] X. Kong, J. Deng, L. Li, Y. Liu, X. Ding, J. Sun, and J. Z. Liu, Tunable auxetic properties in group-IV monochalcogenide monolayers, Phys. Rev. B **98**, 184104 (2018).

[46] K. E. Evans, M. A. Nkansah, I. J. Hutchinson, and S. C. Rogers, Molecular network design, Nature (London) **353**, 124 (1991).

[47] A. Yeganeh-Haeri, D. J. Weidner, and J. B. Parise, Elasticity of α-cristobalite: A silicon dioxide with a negative poisson's ratio, Science **257**, 650 (1992).

[48] D. Vanderbilt and R. D. King-Smith, Electric polarization as a bulk quantity and its relation to surface charge, Phys. Rev. B **48**, 4442 (1993).

[49] N. A. Spaldin, A beginner's guide to the modern theory of polarization, J. Solid State Chem. **195**, 2 (2012).

[50] See Supplemental Material at http://link.aps.org/supplemental/10.1103/PhysRevB.109.035204 for Tables SI-SIII, Figures S1-S8, and supplemental discussions.

[51] H. Liu, A. T. Neal, Z. Zhu, Z. Luo, X. Xu, D. Tománek, and P. D. Ye, Phosphorene: An unexplored 2D semiconductor with a high hole mobility, ACS Nano **8**, 4033 (2014).

[52] N. Marzari, A. A. Mostofi, J. R. Yates, I. Souza, and D. Vanderbilt, Maximally localized wannier functions: theory and applications, Rev. Mod. Phys. **84**, 1419 (2012).

[53] N. Marzari and D. Vanderbilt, Maximally localized generalized wannier functions for composite energy bands, Phys. Rev. B **56**, 12847 (1997).

[54] L.-X. Zhao and J. Liu, Piezoelectricity in binary wurtzite semiconductors: A first-principles study, Appl. Phys. Express **14**, 121003 (2021).

[55] E. J. Skoug and D. T. Morelli, Role of lone-pair electrons in producing minimum thermal conductivity in nitrogen-group chalcogenide compounds, Phys. Rev. Lett. **107**, 235901 (2011).